ACS APPLIED MATERIALS & INTERFACES

RESEARCH ARTICLE

www.acsami.org

Fluorinated and Nanoporous Graphene Materials As Sorbents for Gas Separations

Joshua Schrier*

Department of Chemistry, Haverford College, Haverford, Pennsylvania 19041, United States

Supporting Information

ABSTRACT: The physisorption of gases on surfaces depends on the electrostatic and dispersion interactions with adsorbates. The former can be tuned by introducing charge variations in the material, and the latter can be tuned by chemical substitution. Using atomistic Monte Carlo calculations, the Henry's law constants, and isosteric heats of adsorption of CH_4, CO_2, N_2, O_2, H_2S, SO_2, and H_2O on graphene, two-dimensional polyphenylene (2D-PP), fluorographene, and fluoro(2D-PP) surfaces are used to demonstrate the tunability of these two types of interaction. With the exception of H_2O, fluorination and nanoporosity-induced charge variations reduce the binding of the adsorbates. Gas separations relevant for CO_2 sequestration, biogas upgrading, SO_2 pollution control, and air dehumidification are considered, and in most cases, the nanoporosity and fluorination reduce the selectivity of adsorption. The exceptions are separations involving adsorption of H_2O and the SO_2/N_2 separation, where the large dipole moments of the adsorbed species leads to enhanced binding relative to the nonpolar species.

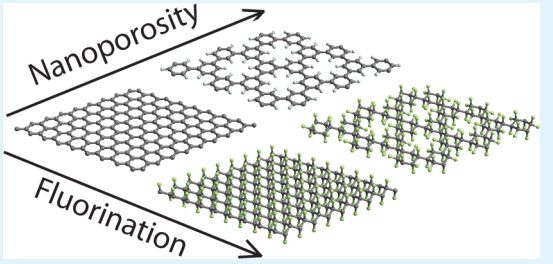

KEYWORDS: porous graphene, fluorographene, physisorption, Monte Carlo, gas separation

INTRODUCTION

Activated carbon sorbents are used for many chemical separations.[1,2] However, because they are amorphous, and the precise atomistic surface details are unknown, it is necessary to construct models for these structures to simulate and understand gas adsorption.[3−5] An alternative is to consider simpler carbon nanotubes and graphene as model structures for simulations and laboratory studies. Besides the conceptual simplicity of considering a tubular or planar geometry, these materials are interesting in their own right, because the highly ordered pores and confined geometries in carbon nanostructures can be used to enhance gas adsorption and selectivity for specific gases.[6−10] In addition to using carbon nanostructures as model sorbents, gas adsorption on carbon nanotubes is also of interest for chemical sensor applications[11] and doping of semiconductor nanotubes for electronics applications.[12] Although the adsorption of gases on bulk graphite surfaces have been studied for many years,[13−15] only recently has it become possible to study adsorption on a single graphene sheet.[16] Subsequent work has focused primarily on gas sensing, as reviewed by Ratinac et al.,[17] so not much is known about gas adsorption isotherms on graphene, with the exception of experimental studies of ozone[18] and hydrogen[19,20] adsorption. These experimental studies, and recent density functional theory studies of noble gases and water adsorption,[21] indicate that the adsorption on a single graphene sheet differs from adsorption on bulk graphite surfaces. Computational studies of gas adsorption on graphene have used electronic structure calculations to identify the minimum energy geometry and the extent of charge transfer between the sorbate and the graphene surface,[21−27] but these consider only the zero-temperature limit, and not the thermodynamics of the adsorption process at finite temperature.

The present work is motivated by two observations. First, Jiang and Sandler observed that curvature induces a nonuniform charge distribution in C_{168} Schwartzite surfaces, enhancing the selective adsorption of CO_2 (which has a large quadrupole moment) versus N_2 (which has a small quadrupole moment).[6] This paper investigates an alternative route to introducing charge nonuniformity, by using a nanoporous graphene material such as the two-dimensional polyphenylene (2D-PP) synthesized by Bieri et al.,[28] shown in Figure 1b. Because some carbon atoms are bonded to three carbons and others to two carbons and a hydrogen, the charges will not be uniform, which may enhance the interaction with polar adsorbate molecules. Second, this paper investigates the extent to which nonselective dispersion interactions can be reduced by fluorinating the material. Because fluorine is not very polarizable, its dispersion interaction is generally weak. Moreover, the polar C−F bond may provide additional nonuniformity of the charge distribution, further enhancing the adsorption of polar molecules. Fluorinated graphene (fluorographene), shown in Figure 1c, has been synthesized by several research groups,[29−32] and is both thermally stable at up to

Received: August 22, 2011
Accepted: October 21, 2011
Published: October 21, 2011

dx.doi.org/10.1021/am2011349 | ACS Appl. Mater. Interfaces 2011, 3, 4451–4458

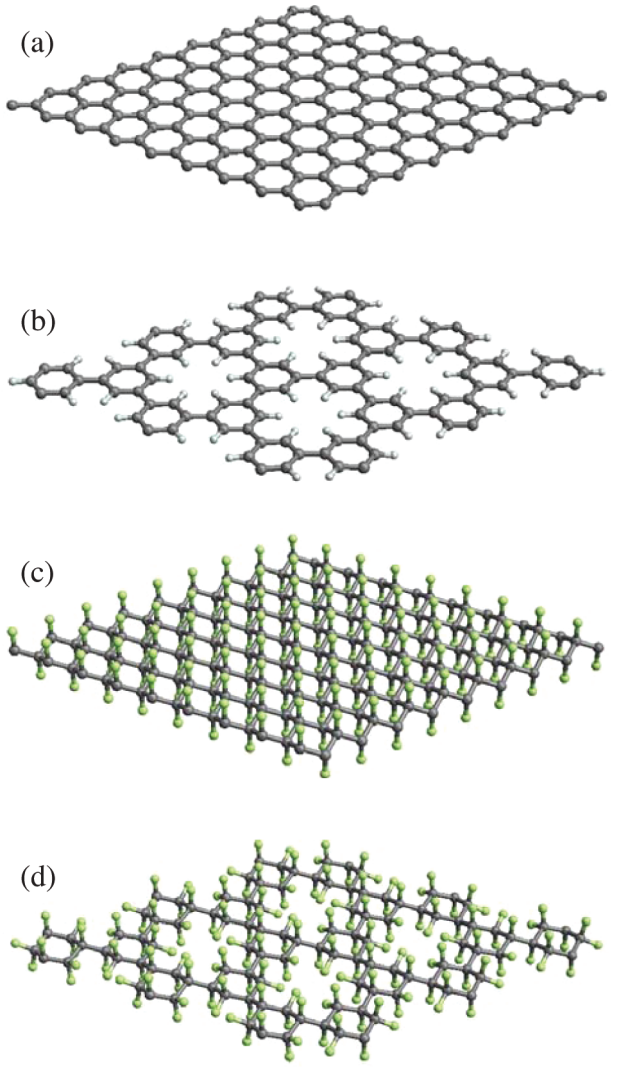

Figure 1. PM6-D2 optimized geometries of sorbents considered in this work: (a) Graphene; (b) two-dimensional polyphenylene (2D-PP) ; (c) fluorographene; (d) fluoro(2D-PP).

400 °C in air[30] and chemically inert (it is essentially a two-dimensional generalization of polytetrafluoroethylene, i.e.,"Teflon"). Thus, an additional practical advantage of fluorinated-graphene based sorbents is resistance to chemical degradation by reactive species in the gas stream being purified, e.g., the sulfuric acid produced by SO_2 and H_2O in flue gas. Finally, these sorbents can be made in the laboratory. Graphene, 2D-PP,[28] and fluorographene[29−32] have all been synthesized; fluoro(2D-PP), shown in Figure 1d, could be synthesized by reacting 2D-PP with XeF_2 gas, similar to the conversion of graphene and graphane to fluorographene,[29,30] or with SF_6 plasma.[33] Unlike the use of nanoporous graphenes as filter-like membranes for gas separation,[34−37] there is no need for the film to be contiguous and unbroken. The only requirement is that a sufficiently large surface area is exposed. Consequently, the graphene patchwork structures reviewed by Eda and Chhowalla[38] would be sufficient so long as the surface was accessible to the gas phase adsorbates.

This paper describes calculations of the Henry's law constants and isosteric heats of adsorption for CH_4, CO_2, N_2, O_2, H_2S, SO_2, and H_2O physisorbing to planar surfaces of graphene, 2D-PP, fluorographene, and fluoro(2D-PP), to explore the hypothesis that atomic-scale nanoporosity and fluorination will enhance the binding of dipolar (H_2O, SO_2, H_2S) and large quadrupolar (CO_2) species, while minimizing the binding of species having only small quadrupoles (N_2, O_2) or lacking dipole- and quadrupole-moments entirely (CH_4) . Though Henry's law is applicable only in the limit of low pressure,[39] and does not take into account interactions between adsorbate molecules that occur at higher pressures and result in nonlinear isotherms, it does provide an initial estimate useful for designing temperature- and pressure-swing adsorption separation processes.[1] From this data, adsorption selectivities of various combinations of these gases are examined, in particular separation of CO_2 and SO_2 from flue gases, purification of natural gas, and removal of H_2O from air.

COMPUTATIONAL METHODS

Sorbent Structure and Charges. The 2D-PP unit cell serves as a building block for constructing the geometries of all of the species described here, as it can be considered as a generalization of graphene in which some of the carbons have been replaced by hydrogen atoms. In all cases, a 3 × 3 supercell (corresponding to edge lengths of 22−24 Å) was used for the simulations, unless otherwise noted. These supercells are shown in Figure 1. For the fluorinated species, the "chair" arrangement of the fluorine atoms was used, as this is the lowest energy configuration in several density-functional theory (DFT) calculations.[40−42] The atom coordinates and supercell lattice constants were optimized using PM6-D2[43,44] semiempirical Hartree−Fock theory with empirical dispersion correction terms, using MOPAC 2009, v11.053 L.[45] These calculations imposed two-dimensional periodic boundary conditions, sampling only the Γ-point in the Brillouin zone; the same *k*-point sampling and 3 × 3 supercell was used in the DFT calculations of 2D-PP by Blankenburg et al.[37]

For graphene, it is unnecessary to obtain the atomic charges, because they are all zero. For fluorographene, the optimized chair-fluorographene coordinates and unit cell of Leenaerts et al.[40] were used for the charge calculations described below. For 2D-PP and fluoro(2D-PP), the atom coordinates of a single unit cell were used, with the unit-cell dimensions obtained by dividing the supercell dimensions by three in both periodic directions. A 16 Å vacuum region was added in the direction perpendicular to the plane of the atoms. DFT calculations with ABINIT 6.4.1,[46] using the Perdew−Burke−Ernzerhof (PBE) generalized gradient exchange correlation functional, norm-conserving Trollier−Martins pseudopotentials, and a planewave energy cutoff of 150 Ry, were performed to obtain the charge density. The Brillouin zone was sampled with a 6 × 6 × 1 Monkhorst−Pack grid (the last being the direction perpendicular to the plane). The resulting charge density was used to perform an iterative-Hirshfeld (Hirshfeld-I)[47] calculation to obtain the atom-centered charges, as described in previous work.[48] The Hirshfeld-I scheme has been demonstrated to yield an accurate electrostatic potential.[49]

Classical Force-Field Parameters. A Lennard−Jones (6−12) plus Coulomb potential was used for both sorbents and adsorbates. The sorbents were described using the Hirshfeld-I charges described above and Lennard-Jones potential parameters from the literature. The graphene carbon atom parameters are from Fileti et al. and the benzene parameters from Fileti et al. were used for the carbon and hydrogen atoms in 2D-PP.[50] For the fluorinated sorbents the carbon and fluorine atom parameters are taken from the fluorocarbon parameters used by Gomes and Padua.[51] The adsorbate Lennard−Jones and charge parameters are all taken from the literature: The SO_2 parameters from Ketko et al.;[52] the H_2S parameters from Nath;[53] the H_2O parameters from the SPC/E model of Berendsen et al.;[54] the CH_4 parameters from the united atom model of Liu and Smit;[55] the N_2, O_2, and CO_2 quadrupolar model

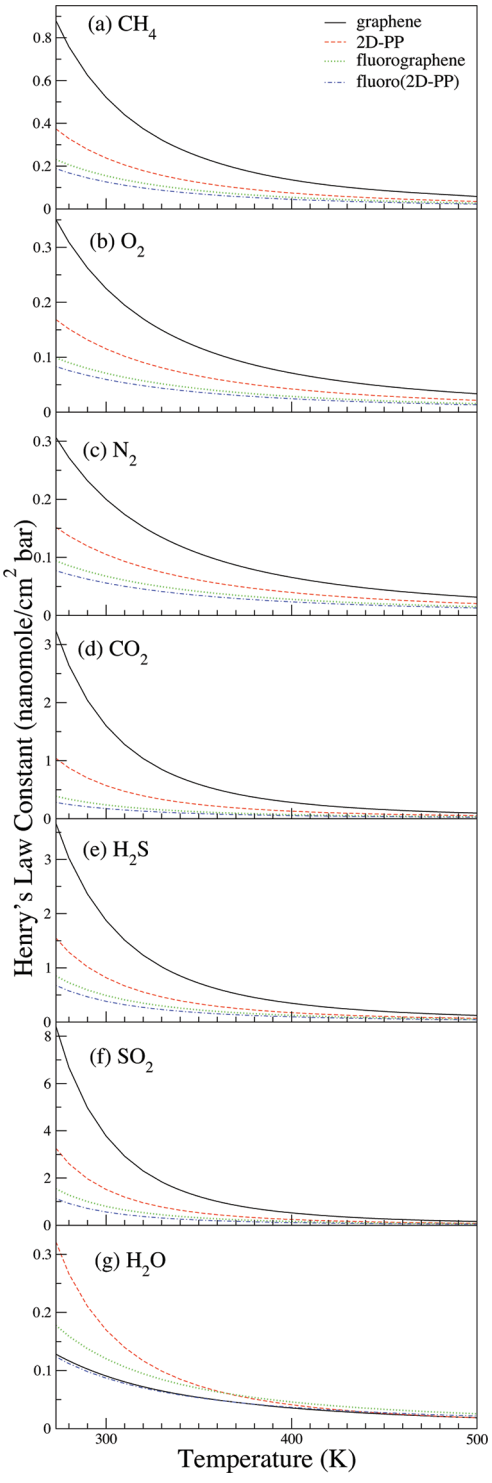

Figure 2. Henry's Law constant for adsorption of gas species on graphene, 2D-PP, fluorographene, and fluoro(2D-PP) surfaces. These values are based on adsorption on only one side of the surface, and should be doubled if both sides of the sorbent surface are exposed to the adsorbate gas.

parameters from Stoll et al.[56] Cross-interactions are described by the Lorentz−Berthelot combining rules. A complete table of the parameters and charges in contained in the Supporting Information. These adsorbate parameters have been previously used to study adsorption processes on carbon nanostructures[9,50] and metal organic frameworks (MOFs).[55,57] These parametrizations were used, rather than comprehensive force-field parametrizations such as UFF or COMPASS, so as to accurately describe the dipole and quadrupole moments of the sorbates, and to accurately describe the sorbate−sorbate interactions needed to reproduce the equations of state for the gases. The former property is necessary for this paper, particularly for testing the hypothesis that nanoporosity and fluorination are effective for separating large quadrupole species (CO_2) from small quadrupole species (N_2, O_2). The latter property does not play a role in the current paper, but does provide a foundation for future simulations studying the pressure-dependent adsorption isotherms, which depend on an accurate description of the gas fugacity.

Determination of Henry's Law Constant. The Henry's Law constants and isosteric heat of adsorption were calculated following the method described by Do et al.[8,58] Denoting the interaction energy between the sorbent and sorbate as $\phi(\vec{r},\omega)$, where $\vec{r}$ and ω are the position and orientation of the sorbate relative to the sorbent surface, the Henry's Law constant with respect to pressure is given by

$$K_P = \frac{1}{AN_A k_B T}\left(\int_\Omega\int_\omega \exp\left[\frac{-\phi(\vec{r},\omega)}{k_B T}\right] d\omega d\vec{r} - \int_\Omega\int_\omega H[-\phi(\vec{r},\omega)] d\omega d\vec{r}\right) \quad (1)$$

where A is area of the sorbent, N_A is Avogadro's constant, k_B is Boltzmann's constant, T is the temperature (in Kelvin), and H is the Heaviside step function. The second term corresponds to the accessible volume in the simulation, and is necessary for keeping the Henry constant positive as discussed by Do et al.[8] The integrals over the positions in the simulation cell volume, Ω, and the possible sorbate orientations, ω, are evaluated using 10^7 Monte Carlo evaluations of random adsorbate position and orientation for each adsorbate and sorbent pair. The sorbent and adsorbates are treated as rigid species. Positions in the direction perpendicular to the sorbent were sampled out to 12 Å. The positions and orientations of the adsorbate were generated using the uniformly distributed Mersenne-Twiser pseudorandom number algorithm in Mathematica 7.0[59] The energy, $\phi(\vec{r},\omega)$, was evaluated using the force field parameters described above, using LAMMPS 2011.02.[60,61] Periodic boundary conditions were imposed in the two dimensions of the sorbent plane. Long-range Coulomb interactions were evaluated using Ewald summation to a precision of 1×10^{-4}; the Lennard−Jones interactions were truncated to a distance of 14.0 Å. Similarly, the isosteric heat of adsorption can be evaluated from

$$q_{st} = k_B T - \frac{\int_\Omega\int_\omega [\phi(\vec{r},\omega)/k_B T]\exp[-\phi(\vec{r},\omega)/k_B T] d\omega d\vec{r}}{AN_A K_P} \quad (2)$$

Results shown in Figures 2−7 were explicitly calculated every 10 K. In all cases, the quadrature error was less than 0.1%; error bars are not clearly visible at the scale of the graphs.

RESULTS AND DISCUSSION

Sorbent Characteristics. The PM6-D2 optimized geometries of the four sorbents are shown in Figure 1, and the Cartesian coordinates are provided in the Supporting Information. For PM6-D2 graphene, the mean C−C bond length is 1.428 Å, which is slightly greater than the experimental 1.422 ± 0.001 Å C−C bond length in graphite measured by Trucano and Chen,[62] and comparable to the 1.427 Å PBE/6-311G* C−C bond length of graphene reported by Avramov et al.[63] For PM6-D2 fluorographene, the mean C−C bond length is 1.513 Å, and the mean C−F bond length is 1.371 Å. This is comparable to the plane-wave pseudopotential PBE DFT results of 1.579 Å and 1.371 Å,

respectively, reported by Leenaerts et al.[40] and the projector-augmented wave (PAW) PBE DFT results of 1.584 Å and 1.382 Å, respectively, reported by Artyukhov and Chernozatonskii.[64] All calculations yield roughly tetrahedral fluorographene bond angles, but the PM6-D2 calculation predicts a mean C−C−C angle of 108.5° and a mean C−C−F angle of 110.4°, compared to 110.8° and 108.1° reported by Leenaerts et al.,[40] and 110.9 and 108.0° reported by Artyukhov and Chernozatonskii.[64] The DFT result are consistent with the MP2/6-31G(d) bond angles for 2-fluoro-2-methyl-propane reported by Yamada and Bozzelli.[65] Moreover, a smaller C−C−F angle is consistent with Bent's rule,[66] since (in the language of valence bond theory) the electronegative F atom increases the p-atomic orbital character in the sp^3 hybrid formed with the central C atom. This is evidence that the C−C−F and C−C−C bond angles are incorrect within the PM6-D2 model chemistry. However, given the similarity of all the results, we conclude that PM6-D2 is a computationally efficient alternative to other electronic structure methods for geometry optimizations of graphene and fluorographene species.

Because of the prohibitively large number of electrons, determination of the Hirshfeld-I charges for the sorbent atoms was performed using only a single unit cell, rather than the entire 3 × 3 supercell. To establish the similarity of the charges in each portion of the supercell, we compared the PM6-D2 Mulliken charges in each of the unit cells of 2D-PP and fluoro(2D-PP). For 2D-PP, the PM6-D2 Mulliken charges vary by at most ±0.001 e^- (±1%) between the equivalent atoms in the 9 replicas of the unit cell, and the mean absolute deviation is 0.0002 e^-. Similarly, for fluoro(2D-PP) the Mulliken charges differ by at most ±0.001 e^- (±2%), and the mean absolute deviation is 0.0002 e^-. This justifies the use of the single-unit cell to compute the Hirshfeld-I charges, and the transferability of these charges in the different regions of the supercell. The 326-atom fluorographene supercell employed here contains C−C−C angles ranging from 108.4−108.8°, and C−C−F angles ranging from 110.3°-110.4°, without the equivalence of the 9 unit cells seen in the 2D-PP and fluoro-(2D-PP) cases. For this reason, the 8-atom unit cell reported by Leenaerts et al.,[40] where all the angles are the same, was used for the assignment of charges. The Hirshfeld-I calculations assign a charge of −0.094 on the fluorine atoms and +0.094 on the carbon atoms, which we assigned to the atoms in the larger supercell.

Adsorption Properties. The computed Henry's law constants for the excess physisorption of gases on the various adsorbates are shown in Figure 2. Note that these values assume adsorption on only one side of the surface, and should be doubled if both sides of the sorbent surface are exposed to the adsorbate gas. With the exception of H_2O (Figure 2g), adsorbate molecules have the largest Henry's law constants when adsorbed to graphene, due to the large dispersive interaction. This is followed by adsorption on 2D-PP, which has a smaller dispersive contribution, and then by fluorographene and fluoro(2D-PP) which have the weakest dispersion interaction. The adsorption of H_2O is an exception to this trend, because it has both the largest dipole moment and a smaller attractive potential-well-depth term than the other species. Consequently, H_2O has the largest Henry's law constant for physisorption on 2D-PP, where the charge fluctuations on the different sites attract the water molecule and the attractive dispersion interaction is still present (although weaker than in graphene).

The computed isosteric heats of adsorption are shown in Figure 3. As with the Henry's Law constant, adsorbate molecules have the largest heat of adsorption on graphene, and the weaker

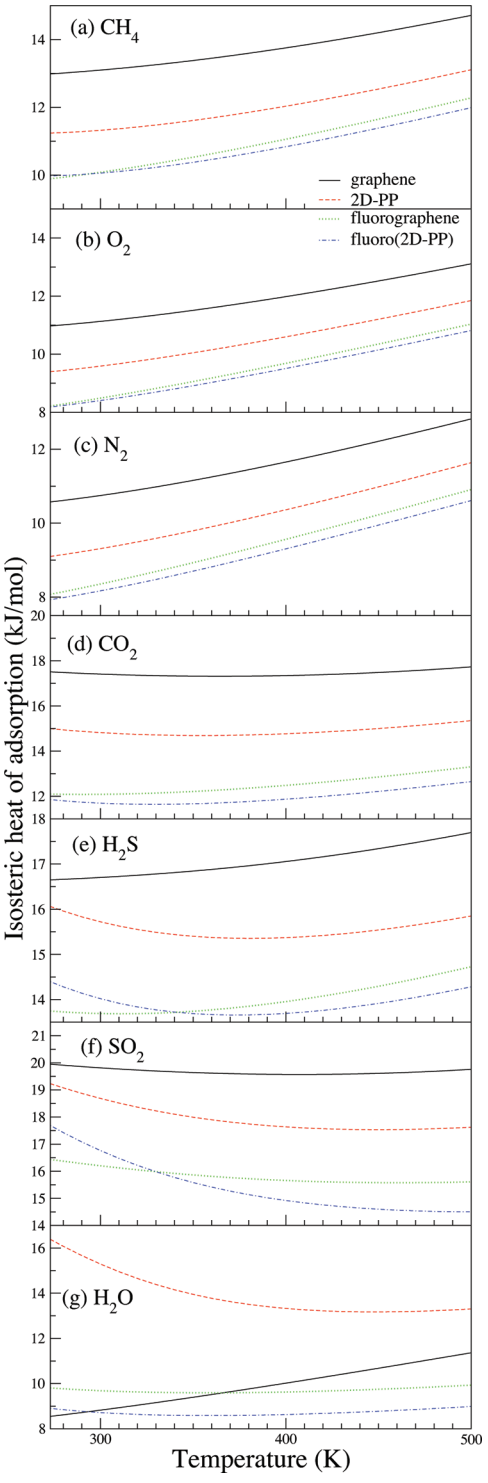

Figure 3. Isosteric heats of adsorption for the gas species on graphene, 2D-PP, fluorographene, and fluoro(2D-PP) surfaces.

dispersive interaction with the fluorinated sorbents leads to smaller heats of adsorption. Again, the exception is H_2O (Figure 3g), which has the largest heat of adsorption on 2D-PP, for the same reasons that its Henry's law constant is the largest. The isosteric heats of adsorption on the planar graphitic surfaces are less than those on curved graphitic surfaces,[67] which is why the heats of adsorption are smaller than those reported for adsorption in

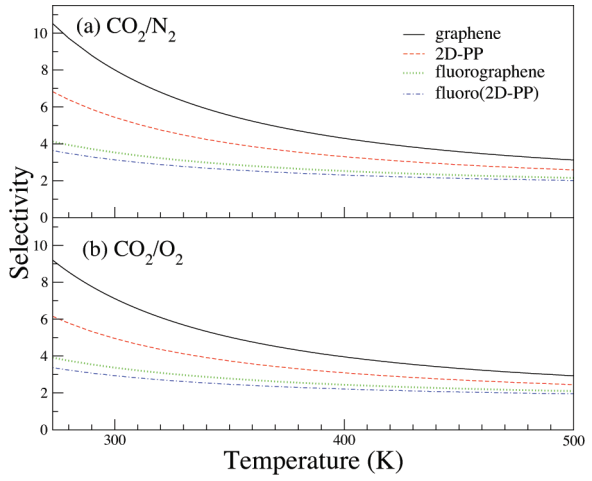

Figure 4. Adsorption selectivity ratios relevant to CO_2 separation. (a) CO_2/N_2 and (b) CO_2/O_2.

C_{168} Schwartzite by Jiang and Sandler.[6] For comparison, the isosteric heats of adsorption of CO_2 and CH_4 on zeolites and MOFs are in the range of 14−25 and 10−20 kJ/mol, respectively.[68]

Nonlinearities of the heat of adsorption as a function of temperature arise from the role of orientation, as was previously observed for gas adsorption on carbon nanotubes by Do et al.[8] The nonlinearity is most pronounced for polar molecules (H_2S, SO_2 and H_2O) interacting with the charge-varying surfaces (2D-PP, fluorographene, and fluoro(2D-PP) surfaces), because it is in these cases that the interaction energy varies the most as a function of the molecule orientation. In the case of CH_4, O_2, and N_2 (shown in Figure 3a−c), the heats of adsorption increase monotonically with temperature. Since CH_4 is treated with a single-site united atom model, it has no orientation dependence, and the orientation dependence is small for the weak quadrupolar species O_2 and N_2. For the solely dispersive interaction with graphene, the heat of adsorption either increases or stays essentially constant.

Potential Applications. To ascertain the potential applications of these materials, we will discuss the selectivity of adsorption relevant to various industrial gas mixtures. The selectivity (also known as the separation factor) for component A relative to component B is defined as the dimensionless quantity (x_A/x_B)-(y_B/y_A) where x_i and y_i are the mole fractions of component i in the adsorbed and gaseous phases, respectively. The selectivity is a measure of the relative adsorption of different species to a surface, hence a larger selectivity is more desirable because it requires fewer process steps to obtain pure components, simplifying the separation procedure. For the (linear) Henry's law isotherm, the selectivity reduces to the ratio of the Henry's law constants of the two species, and is partial- and total-pressure independent because the reference (nonadsorbed) gases are in the low-pressure ideal limit. Consequently, this does not take into account the interactions between adsorbate molecules, nor competition for the adsorption sites, which may occur at high pressure.

CO_2 separation. Removing CO_2 from combustion gases is a topic of great scientific interest, and the reader is referred to recent reviews of the various alkanolamine solutions, ionic liquids, zeolites, MOFs, and basic resins that have been investigated for this application.[69−72] Previous calculations addressing

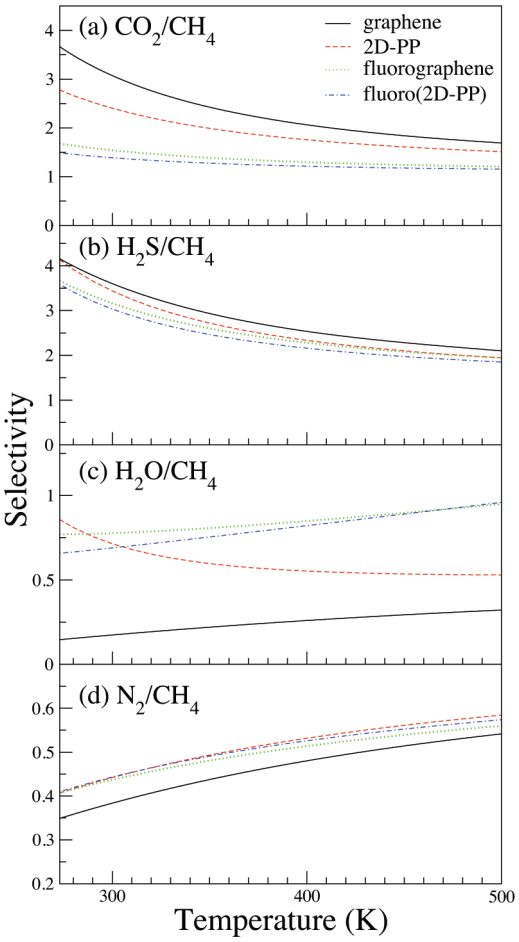

Figure 5. Adsorption selectivity ratios relevant to natural gas purification and upgrading. (a) CO_2/CH_4; (b) H_2S/CH_4; (c) H_2O/CH_4; (d) N_2/CH_4 .

the use of carbon nanostructures for this separation of CO_2 from N_2 include the work by Montoya,[73] and the work of Jiang and Sandler[6] discussed in the Introduction. Calculations by Liu and Wilcox have also investigated the use of carbon for long-term geological CO_2 storage.[74] There are also several experimental studies of use of activated carbon for this separation.[75−77] Defective graphene sheets can also undergo a chemisorption reaction with CO_2[78] but this is outside of the current investigation.

Examining the results of Figure 4, graphene shows the largest selectivity for CO_2 adsorption against both N_2 and O_2. The selectivities for the planar graphene surface considered here are less than that of the curved surfaces examined by Jiang and Sandler.[6] The selectivity for CO_2 decreases for 2D-PP, indicating that curvature is more effective for selectively adsorbing quadrupolar species than nanoporosity. The selectivity for CO_2 decreases further for fluorographene and fluoro-(2D-PP). Therefore, fluorination is not an effective strategy for enhancing the selective adsorption of strongly quadrupolar species over weakly quadrupolar species, as the dispersion interaction dominates the interaction in all cases. However, the fluorinated sorbents have selectivities between 2 and 4, which are comparable to the room temperature CO_2/N_2 adsorption selectivity at low pressure of 3.5 for MOF-5,[79] but lower than the selectivities of around 10 for MIL-47 and IRMOF-11,[68] and 54 for zeolite 13X.[80]

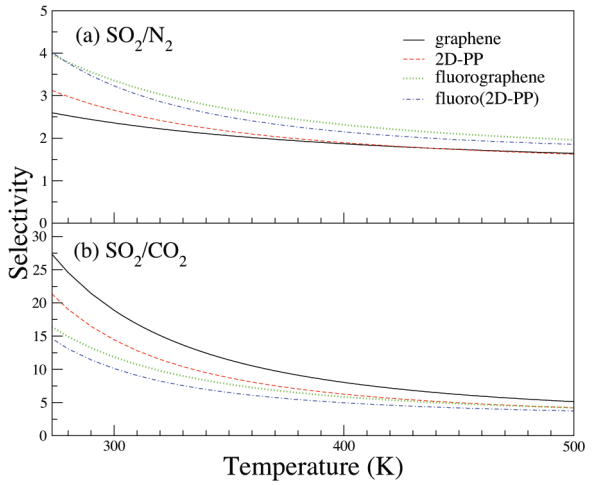

Figure 6. Adsorption selectivity ratios relevant to postcombustion SO_2 pollution control. (a) SO_2/N_2 and (b) SO_2/CO_2.

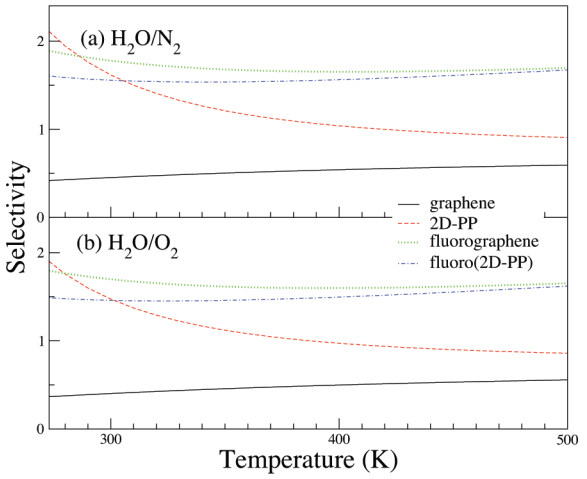

Figure 7. Adsorption selectivity ratios relevant to dehumidification of air. (a) H_2O/N_2 and (b) H_2O/O_2.

Biogas Upgrading. A second application is the upgrading of "biogas", a mixture of CH_4, CO_2, and N_2 saturated with H_2O vapor, produced by anaerobic digestion of organic matter in landfills and manure pits.[81] Removing the CO_2, N_2, and H_2O increases the caloric value of the gas, and makes it compatible with municipal natural gas infrastructure requirements. Palmer et al. have recently reported Grand-Canonical Monte Carlo (GCMC) calculations on the role of pore morphology and size distributions in realistic atomistic models of amorphous carbons for separation of CO_2/CH_4 mixtures, which they compared to planar "slit pore" and SWCNT pores.[10] Biogas also typically includes H_2S, most of which is removed by reaction with iron oxide, but it is also desirable to remove the remaining trace amounts.[81] Metal organic frameworks have been proposed for this application,[82] as have single-wall carbon nanotubes.[9]

Figure 5 shows the selectivity of adsorption of the CO_2, H_2S, and H_2O from CH_4. The quadrupole interaction plays a relatively small effect in the CO_2 physisorption which is otherwise dominated by dispersion interactions, so the CO_2/CH_4 selectivity is greatest on graphene, and is reduced for the fluorinated species. In comparison, the CO_2/CH_4 selectivity of the Cu(hfipbb)$(H_2hfipbb)_{0.5}$ MOF is around 2.5 at room temperature in the low pressure limit, and increases to around 4 at high pressure.[83] Similarly, CUBTC, IMOF-1 and MOF-5 have CO_2/CH_4 selectivities <2 at room temperature in the low pressure limit.[79,84]

For the case of H_2S/CH_4 separation shown in Figure 5b, the electrostatic and dispersive interactions are comparable, leading to similar selectivities for all the sorbents. The selectivity of the planar surfaces considered in this work are much lower than the selectivities of 10−100 predicted for single-wall carbon nanotube arrays recently reported by Wang et al.[9] For the case of H_2O, shown in Figure 5c, the selectivities are all less than one, i.e., CH_4 is preferentially adsorbed on the surface rather than H_2O. However, this is weakest for fluorographene and fluoro(2D-PP), consistent with the Henry's law constant trends in Figure 2g. Similarly, for the case of N_2 shown in Figure 5d, the selectivities are also less than one, indicating preferential adsorption of CH_4 on all of the materials. The quadrupole moment of N_2 causes it to bind more strongly to the porous and fluorinated sorbants than to graphene, because of the electrostatic interaction with the charges in the sorbent surface.

SO_2 Pollution Control. Combustion of coal results in SO_2, an air pollutant contributing to acid rain, which must be removed from the flue gas mixture of CO_2 and N_2. The selectivities relevant to this separation are shown in Figure 6. For selective adsorption of SO_2/N_2, the fluorinated sorbents have greater selectivity for SO_2 adsorption. For selective adsorption of SO_2/CO_2, while the graphene surface displays the highest selectivity, the fluorinated surfaces are still highly selective for SO_2 adsorption. Although the SO_2 adsorption selectivities of single-wall carbon nanotubes computed by Wang et al.[9] are higher than the planar surfaces considered here, carbon nanotubes are probably not useful sorbents. Quantum chemistry calculations have shown that chemisorption occurs on carbon surfaces (such as those of graphene and carbon nanotubes), leading to reduction of SO_2 to elemental sulfur, and oxidation of the graphene sorbent to carbon dioxide.[85] Fluorographene and fluoro(2D-PP) sorbents would resist degradation resulting from chemisorption.

Air Dehumidification. The final application is removal of H_2O from air, shown in Figure 7. The qualitative difference between the fluorinated and nonfluorinated sorbents arise from water having the largest dipole moment versus N_2 and O_2 having only a weak quadrupole and otherwise interacting with the surface primarily through dispersive interactions. In both cases, graphene shows a selectivity less than one, i.e., preferential binding of N_2 and O_2 as opposed to H_2O. This is consistent with the overall larger attractive dispersion contribution of the O_2 and N_2 molecule Lennard-Jones parameters as compared to that of H_2O. Introducing charge variations alters the balance between the interactions: 2D-PP shows selectivity greater than one at low temperatures, and selectivity less than one at high temperatures. Substantially reducing the dispersion interaction, leads to both fluorographene and fluoro(2D-PP) showing preferential adsorption of H_2O throughout the temperature range. Although the selectivity is low, it is qualitatively different from the unmodified graphene sorbent.

CONCLUSION

Molecular simulations have been used to investigate the effect of nanoporous structuring and fluorination of graphene surfaces on the adsorption of CH_4, CO_2, N_2, O_2, H_2S, SO_2, and H_2O. Introducing nanoscale pores (as in 2D-PP) leads to a nonuniform

charge distribution which increases electrostatic interactions with adsorbate molecules, particularly those with large dipole moments, but the effect on the interaction with most adsorbate molecules is typically small compared to the dispersion interaction. Fluorination (as in fluorographene and fluoro(2D-PP)) reduces the attractive dispersion interactions which play the largest role in the adsorption of nonpolar molecules. With the exception of H_2O, the strongest contribution to physisorption on the surface is via the dispersion interaction, with electrostatics playing a secondary role. This is manifested by the reduced Henry's law constants for the fluorinated and nanoporous sorbents. H_2O is exceptional in that it has both a large dipole moment and a small attractive dispersion term in the SPC/E potential model used here, thus favoring the additional electrostatic interactions with 2D-PP. Using the Henry's law constants, the adsorption selectivity was calculated for several industrial gas separations. In most cases, the selectivity is greatest for unmodified graphene surfaces and is reduced by introduction of nanoporosity and fluorination. The exceptions are separations involving adsorption of H_2O and the SO_2/N_2 separation, where the large dipole moments of the adsorbed species leads to enhanced binding relative to the nonpolar species.

■ ASSOCIATED CONTENT

Supporting Information. Tables of Lennard−Jones parameters and sorbent surface Cartesian coordinates and charges. This material is available free of charge via the Internet at http://pubs.acs.org/

■ AUTHOR INFORMATION

Corresponding Author
*E-mail: jschrier@haverford.edu.

■ ACKNOWLEDGMENT

I thank Anna Brockway for performing the ABINIT and Hirshfeld-I calculations and for her careful reading of the manuscript, and Dr. Ortwin Leenaerts (Univ. Antwerpen) for providing the fluorographene coordinates reported in ref 40. This work was partially supported by the Donors of the American Chemical Society Petroleum Research Fund and Research Corporation for Science Advancement's Cottrell Scholar grant. This work used resources of the National Energy Research Scientific Computing Center, which is supported by the Office of Science of the U.S. Department of Energy under Contract DE-AC02-05CH11231.

■ REFERENCES

(1) Yang, R. T. *Gas Separation by Adsorption Processes*; Imperial College Press: London, 2008.
(2) Sircar, S.; Golden, T. C.; Rao, M. B. *Carbon* **1996**, *34*, 1–12.
(3) Robertson, J. *Adv. Phys.* **1986**, *35*, 317.
(4) Jain, S. K.; Pellenq, R. J.-M.; Pikunic, J. P.; Gubbins, K. E. *Langmuir* **2006**, *22*, 9942.
(5) Nguyen, T. X.; Cohaut, N.; Bae, J.-K.; Bhatia, S. K. *Langmuir* **2008**, *24*, 7912.
(6) Jiang, J.; Sandler, S. I. *J. Am. Chem. Soc.* **2005**, *127*, 11989.
(7) Huang, L.; Zhang, L.; Shao, Q.; Lu, L.; Lu, X.; Jiang, S.; Shen, W. *J. Phys. Chem. C* **2007**, *111*, 11912–11920.
(8) Do, D. D.; Do, H. D.; Wongkoblap, A.; Nicholson, D. *Phys. Chem. Chem. Phys.* **2008**, *10*, 7293.
(9) Wang, W.; Peng, X.; Cao, D. *Environ. Sci. Technol.* **2011**, *45*, 4832.
(10) Palmer, J. C.; Moore, J. D.; Roussel, T. J.; Brennan, J. K.; Gubbins, K. E. *Phys. Chem. Chem. Phys.* **2011**, *13*, 3985.
(11) Wang, Y.; Yeow, J. T. W. *J. Sensors* **2009**, *2009*, 493904–493928.
(12) Liu, S.; Shen, Q.; Cao, Y.; Gan, L.; Wang, Z.; Steigerwald, M. L.; Guo, X. *Coord. Chem. Rev.* **2010**, *254*, 1101–1116.
(13) Lamb, A. B.; Ohl, E. N. *J. Am. Chem. Soc.* **1938**, *60*, 1287.
(14) Bojan, M. J.; Steele, W. A. *Langmuir* **1987**, *3*, 116.
(15) Bojan, M. J.; Steele, W. A. *Langmuir* **1987**, *3*, 1123.
(16) Schedin, F.; Geim, A. K.; Morozov, S. V.; Hill, E. W.; Blake, P.; Katsnelson, M. I.; Novoselov, K. S. *Nat. Mater.* **2007**, *6*, 652.
(17) Ratinac, K. R.; Yang, W.; Ringer, S. P.; Braet, F. *Environ. Sci. Technol.* **2010**, *44*, 1167.
(18) Lee, G.; Lee, B.; Kim, J.; Cho, K. *J. Phys. Chem. C* **2009**, *113*, 14225.
(19) Ma, L.-P.; Wu, Z.-S.; Li, J.; Wu, E.-D.; Ren, W.-C.; Cheng, H.-M. *Int. J. Hydrogen Energy* **2009**, *34*, 2329.
(20) Wang, L.; Stuckert, N. R.; Yang, R. T. *AIChE J.* **2011**, *57*, 2902.
(21) Ambrosetti, A.; Silvestrelli, P. L. *J. Phys. Chem. C* **2011**, *115*, 3695.
(22) Leenaerts, O.; Partoens, B.; Peeters, F. M. *Phys. Rev. B* **2008**, *77*, 125416.
(23) Huang, B.; Li, Z.; Liu, Z.; Zhou, G.; Hao, S.; Wu, J.; Gu, B.-L.; Duan, W. *J. Phys. Chem. C* **2008**, *112*, 13442.
(24) Leenaerts, O.; Partoens, B.; Peeters, F. M. *Microelectron. J.* **2009**, *40*, 860.
(25) Lee, G.; Lee, B.; Kim, J.; Cho, K. *J. Phys. Chem. C* **2009**, *113*, 14225.
(26) AlZahrani, A. Z. *Appl. Surf. Sci.* **2010**, *257*, 807.
(27) Umadevi, D.; Sastry, G. N. *J. Phys. Chem. C* **2011**, *115*, 9656.
(28) Bieri, M.; Trier, M.; Cai, J.; Aït-Mansour, K.; Ruffieux, P.; Gröning, O.; Gröning, P.; Kastler, M.; Rieger, R.; Feng, X.; Müllen, K.; Fasel, R. *Chem. Commun.* **2009**, 6919.
(29) Robinson, J. T.; Burgess, J. S.; Junkermeier, C. E.; Badescu, S. C.; Reinecke, T. L.; Perkins, F. K.; Zalalutdniov, M. K.; Baldwin, J. W.; Culbertson, J. C.; Sheehan, P. E.; Snow, E. S. *Nano Lett.* **2010**, *10*, 3001.
(30) Nair, R. R.; et al. *Small* **2010**, *6*, 2877.
(31) Zbořil, R.; Karlický, F.; Bourlinos, A. B.; Steriotis, T. A.; Stubos, A. K.; Georgakilas, V.; Šafářová, K.; Jančík, D.; Trapalis, C.; Otyepka, M. *Small* **2010**, *6*, 2885.
(32) Cheng, S.-H.; Zou, K.; Okino, F.; Gutierrez, H. R.; Gupta, A.; Shen, N.; Eklund, P. C.; Sofo, J. O.; Zhu, J. *Phys. Rev. B* **2010**, *81*, 205435.
(33) Yang, H.; Chen, M.; Zhou, H.; Qui, C.; Hu, L.; Yu, F.; Chu, W.; Sun, S.; Sun, L. *J. Phys. Chem. C* **2011**, *115*, 16844.
(34) Jiang, D.; Cooper, V. R.; Dai, S. *Nano Lett.* **2009**, *9*, 4019.
(35) Li, Y.; Zhou, Z.; Shen, P.; Chen, Z. *Chem. Commun.* **2010**, *46*, 3672.
(36) Schrier, J. *J. Phys. Chem. Lett.* **2010**, *1*, 2284.
(37) Blankenburg, S.; Bieri, M.; Fasel, R.; Müllen, K.; Pignedoli, C. A.; Passerone, D. *Small* **2010**, *6*, 2266.
(38) Eda, G.; Chhowalla, M. *ACS Nano* **2011**, *5*, 4265–4268.
(39) McQuarrie, D. A.; Simon, J. D. *Physical Chemistry: A Molecular Approach*; University Science Books: Sausalito, CA, 1997.
(40) Leenaerts, O.; Peelaers, H.; Hernández-Nieves, A. D.; Partoens, B.; Peeters, F. M. *Phys. Rev. B* **2010**, *82*, 195436.
(41) Samarakoon, D. K.; Chen, Z.; Nicolas, C.; Wang, X.-Q. *Small* **2011**, *7*, 965.
(42) Sahin, H.; Topsakal, M.; Ciraci, S. *Phys. Rev. B* **2011**, *83*, 115432.
(43) Stewart, J. J. P. *J. Mol. Model.* **2007**, *13*, 1173–1213.
(44) Korth, M.; Pitonák, M.; Rezác, J.; Hobza, P. *J. Chem. Theory. Comput.* **2010**, *6*, 344–352.
(45) Stewart, J. J. P. *MOPAC2009, Version 11.053L*; http://OpenMOPAC.net.
(46) Gonze, X.; et al. *Comput. Phys. Commun.* **2009**, *180*, 2582–2615.
(47) Bultinck, P.; Van Alsenoy, C.; Ayers, P. W.; Carbó-Dorca, R. *J. Chem. Phys.* **2007**, *126*, 144111.

(48) Glor, E. C.; Blau, S. M.; Yeon, J.; Zeller, M.; Halasyamani, P. S.; Schrier, J.; Norquist, A. J. *J. Solid State Chem.* **2011**, *184*, 1445.
(49) Van Damme, S.; Bultinck, P.; Fias, S. *J. Chem. Theory Comput.* **2009**, *5*, 334.
(50) Fileti, E. E.; Dalpian, G. M.; Rivelino, R. *J. Appl. Phys.* **2010**, *108*, 113527.
(51) Gomes, M. F. C.; Pádua, A. A. H. *J. Phys. Chem. B* **2003**, *107*, 14020.
(52) Ketko, M. H.; Kamath, G.; Potoff, J. J. *J. Phys. Chem. B* **2011**, *115*, 4949.
(53) Nath, S. K. *J. Phys. Chem. B* **2003**, *107*, 9498.
(54) Berendsen, H. J. C.; Grigera, J. R.; Straatsma, T. P. *J. Phys. Chem.* **1987**, *91*, 6269.
(55) Liu, B.; Smit, B. *J. Phys. Chem. C* **2010**, *114*, 8515.
(56) Stoll, J.; Vrabec, J.; Hasse, H. *AIChE J.* **2003**, *49*, 2187.
(57) Williams, J. J.; Wiersum, A. D.; Seaton, N. A.; Düren, T. *J. Phys. Chem. C* **2010**, *114*, 18538.
(58) Do, D. D.; Nicholson, D.; Do, H. D. *J. Colloid Interface Sci.* **2008**, *324*, 15.
(59) *Mathematica Version 7.0.1.0*; Wolfram Research, Inc.: Champaign, IL, 2008.
(60) Plimpton, S. *J. Comput. Phys.* **1995**, *117*, 1–19.
(61) http://lammps.sandia.gov.
(62) Trucano, P.; Chen, R. *Nature* **1975**, *258*, 136.
(63) Avramov, P. V.; Sakai, S.; Entani, S.; Matsumoto, Y.; Naramoto, H. *Chem. Phys. Lett.* **2011**, *508*, 86–89.
(64) Artyukhov, V. I.; Chernozatonskii, L. A. *J. Phys. Chem. A* **2010**, *114*, 5389.
(65) Yamada, T.; Bozzelli, J. W. *J. Phys. Chem. A* **1999**, *103*, 7373–7379.
(66) Bent, H. A. *Chem. Rev.* **1961**, *61*, 275–311.
(67) Liu, J.; LeVan, M. D. *Carbon* **2009**, *47*, 3415.
(68) Liu, B.; Smit, B. *Langmuir* **2009**, *25*, 5918.
(69) Düren, T.; Bae, Y.-S.; Snurr, R. Q. *Chem. Soc. Rev.* **2009**, *38*, 1237.
(70) Choi, S.; Drese, J. H.; Jones, C. W. *ChemSusChem* **2009**, *2*, 796.
(71) Hedin, N.; Chen, L.; Laaksonen, A. *Nanoscale* **2010**, *2*, 1819.
(72) D'Alessandro, D. M.; Smit, B.; Long, J. R. *Angew. Chem., Int. Ed.* **2010**, *49*, 6058.
(73) Montoya, A. *Carbon* **2003**, *41*, 29.
(74) Liu, Y.; Wilcox, J. *Environ. Sci. Technol.* **2011**, *45*, 809.
(75) Siriwardane, R. V.; Shen, M.-S.; Fisher, E. P.; Poston, J. A. *Energy Fuels* **2001**, *15*, 279–284.
(76) Radosz, M.; Hu, X.; Krutkramelis, K.; Shen, Y. *Ind. Eng. Chem. Res.* **2008**, *47*, 3783–3794.
(77) Dutcher, B.; Adidharma, H.; Radosz, M. *Ind. Eng. Chem. Res.* **2011**, *50*, 9696.
(78) Cabrera-Sanfelix, P. *J. Phys. Chem. A* **2009**, *113*, 493.
(79) Keskin, S.; Sholl, D. S. *Ind. Eng. Chem. Res.* **2009**, *48*, 914.
(80) Ho, M. T.; Allinson, G. W.; Wiley, D. E. *Ind. Eng. Chem. Res.* **2008**, *47*, 4883–4890.
(81) Knaebel, K. S.; Reinhold, H. E. *Adsorption* **2003**, *9*, 87.
(82) Cavenati, S.; Grande, C. A.; Rodrigues, A. E.; Kiener, C.; Müller, U. *Ind. Eng. Chem. Res.* **2008**, *47*, 6333.
(83) Watanabe, T.; Keskin, S.; Nair, S.; Sholl, D. S. *Phys. Chem. Chem. Phys.* **2009**, *11*, 11389.
(84) Keskin, S.; Sholl, D. S. *Langmuir* **2009**, *25*, 11786.
(85) Pliego, J. R.; Resende, S. M.; Humeres, E. *Chem. Phys.* **2005**, *314*, 127.